

Solidification and melting of cetane confined in the nanopores of silica gel

E. Illeková · M. Miklošovičová · O. Šauša ·
D. Berek

3rd Joint Czech-Hungarian-Polish-Slovak Thermoanalytical Conference Special Chapter
© Akadémiai Kiadó, Budapest, Hungary 2011

Abstract Synthetic silica gels with six different effective diameters of nano-pores (3–30 nm) were loaded with *n*-hexadecane (cetane) after the elimination of adsorbed water. Kinetics of the solidification and melting of cetane was studied by differential scanning calorimetry (DSC) above the room temperature. Two thermodynamically different states of cetane were found in the samples: the free (bulk)-cetane state and the confined-cetane state. As suspected, the third state of cetane can be amorphous. This has been indicated by the small total transformation heat. The complex crystallization effect of cetane has been found to obey the nucleation-and-growth kinetics and also to depend on the dimensions of confining pores of silica gel. The melting of cetane seems to vary only with the average diameter of silica gel pores, which satisfies the Gibbs–Thompson relation. The presented results validate the applicability of the DSC technique for the porometry. The cetane-medium calibration curve for the silica gel nano-thermoporometry has been determined.

Keywords Kinetics · DSC · Confined systems · Nanopores · Cetane · Melting · Solidification

Introduction

Hexadecane (also called cetane) is a normal alkane hydrocarbon with the chemical formula $C_{16}H_{34}$. It is a liquid at the room temperature. Molar mass of cetane is $226.45 \text{ g mol}^{-1}$, its density is 0.773 g mL^{-1} , boiling point is $287 \text{ }^\circ\text{C}$, and the tabulated melting point is $18 \text{ }^\circ\text{C}$. Cetane ignites very easily under compression (the flash temperature, $T_f = 135 \text{ }^\circ\text{C}$; the autoignition temperature, $T_i = 201 \text{ }^\circ\text{C}$), therefore, it is used as a reference for the combustion quality of diesel fuel and other fuel mixtures [1].

Silica gel is a solid formed by silicon dioxide, SiO_2 . It may contain admixtures of different inorganic and organic substances. Due to the presence of Si–OH groups (silanols), surface of non-modified silica gel is rather polar and well wetted with water. Once saturated with adsorbed water, silica gel can be dried up by heating it to $120 \text{ }^\circ\text{C}$. Chemically bound water can be removed by heating to over $450 \text{ }^\circ\text{C}$ without changes in pore structure. The dehydrated silica gel, however, rapidly absorbs water and silanols are regenerated. Surface area of silica gel is usually measured by the gas (nitrogen or argon) adsorption technique [2]. Average values and distribution of both effective pore diameter and pore volume use to be estimated by the liquid (mercury) porometry [2], while pore volume can also be assessed from bulk density of material (Archimedes method).

In this study, the crystallization and the corresponding melting of cetane have been measured by differential scanning calorimetry (DSC). The first-order phase transition of the pure cetane, also called the bulk- or free-cetane, has been compared with the corresponding behavior of cetane confined in the nanopores (3–30 nm) of the silica gel matrix, which was called the confined-cetane.

E. Illeková (✉) · M. Miklošovičová · O. Šauša
Institute of Physics, Slovak Academy of Sciences, Dúbravská 9,
845 11 Bratislava, Slovakia
e-mail: fyziille@savba.sk

D. Berek
Polymer Institute, Slovak Academy of Sciences, Dúbravská 9,
845 41 Bratislava, Slovakia

Materials and Methods

Cetane of technical grade was supplied by Lachema, Czech Republic. Commercial silica gels were from Eka Chemicals, Sweden (designed as Kromasil), NOMURA Chemicals, Japan (Develosil), SiliCycle, Inc., Canada (SiliaspHERE) and one sample was prepared in the laboratory of Faculty of Natural Sciences, Comenius University, Slovakia (SiO₂ aerogel). Their technical parameters are summarized in Table 1.

The silica gels applied in this study were commercial synthesized porous powders of high purity (B type) designed for high performance liquid chromatography (HPLC). Their particle size is 10 μm and their pore volume depends on effective pore size. It ranges from 0.4 to 0.9 mL g⁻¹; the larger the pore diameter the larger is the pore volume. The surface area of silica gels used in this study ranges from 250 to 500 m² g⁻¹. Evidently, the smaller pores the larger surface area. The materials were prepared from silica sol by non-disclosed, proprietary procedures. After the elimination of water, pores of each silica gel were filled with cetane at ambient temperature under atmospheric pressure. The process of filling was based on the action of capillary forces, which pulled cetane into the pores. The step-by-step procedure of filling was stopped when the first additional micro-volume of cetane made wet the apparently “dry” silica gel with pores just filled with cetane. It was assumed that there is no cetane on the outer silica gel surface. Evidently, the orifices of pores were not completely filled because cetane exhibited the meniscus depression. The partial mass of cetane is in Table 1, too.

Melting and solidification of bulk- and confined-cetane forms was studied by the DSC. Two power compensation instruments were used, namely Perkin-Elmer DSC7 with the intracooler filled with the ethylene glycol (controlled cooling down to 0 °C) and Perkin-Elmer DSC8500 with the automatic intracooler (cooling down to -70 °C). Samples of 15–50 mg mass were encapsulated in aluminum pans without any evacuation. The empty pan for the

reference and the dynamic argon atmosphere (30 mL min⁻¹) were used. Continuous-heating regimes with the heating and cooling rate $\beta = \pm 2$ °C min⁻¹ were applied. By modifying β for 1, 2, 5, 10, 20, 30, 40, and 50 °C min⁻¹ and also by isothermal pre-annealing at annealing temperature, T_a from 15.9 to 20.9 °C, the kinetics of the crystallization were analyzed. Each measuring cycle started at +30 °C and the cool/heat procedure was used. It means that first each sample was slowly cooled sufficiently below the equilibrium freezing temperature of cetane (to 0 or -30 °C) and the solidification was measured; then it was continuously heated up to +30 °C and corresponding melt transitions were detected. The kinetics, especially, the onset and maximum of the DSC peak temperatures being $T_{x,b}$ and $T_{p,b}$, and the transformation enthalpies, ΔH_b for the bulk- and $T_{x,c}$, $T_{p,c}$ and ΔH_c for the confined-cetane were specified. No influence of an eventual aging while storing the samples in the DSC at +30, 0, or -30 °C was observed. Both instruments were calibrated for the heating regimes. The In and Zn standards were used. In the case of DSC8500, also the H₂O standard could be used and the double thermal lag in the cooling regime corrected by adding +2.5 °C. Then, the DSC7 temperature axes were corrected to match the data with the DSC8500 ones by adding of 3.5 °C in the heating regime and +5.9 °C in the cooling regime. The precision of determined data is ± 0.7 °C in the case of DSC7 and ± 0.4 °C in the case of DSC8500 and ± 2 J g⁻¹.

Results and Discussion

The sequence of three cycles (the cooling and heating runs) immediately after each other was always realized in the DSC to consider the reproducibility of the studied processes. Figure 1 shows the results for the pure cetane. The solidification starts at 17.0 °C, however, the temperature $T_{x,b}$ sporadically fluctuates in the interval ± 1.1 °C. At the same time, the shape of the exothermal peak is variable being soft-and-wide (dashed line), steeper-and-narrower

Table 1 Characteristic parameters for HPLC silica gels filled with cetane: mean pore diameter, trademark, coefficient of pore filling, confined-cetane fraction, bulk-cetane fraction, non-transformed cetane fraction (as deduced from the DSC measurements of melting phenomena)

<i>d</i> /nm	Trademark	m_c/m_{total}	Conf %	Bulk %	Missing %
3	Develosil	0.22215	50.78	0	49.22
6	Kromasil				
10	Kromasil	0.43078	51.9	21.73	26.37
12	SiliaspHERE	0.45228	63.09	9.99	26.92
15	SiO ₂ -aerogel	0.71080	34.90	7.73	57.37
30	Kromasil	0.29092	83.00	0	17.00
∞	Pure cetane	1	0	100	0

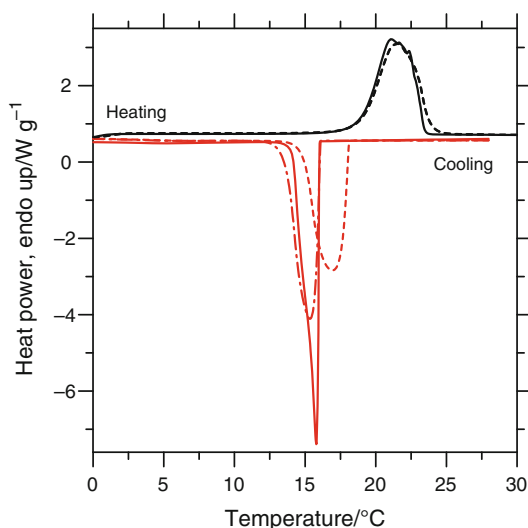


Fig. 1 DSC cooling and heating curves for pure cetane. The scanning rates were $\pm 2 \text{ }^\circ\text{C min}^{-1}$. Full, dashed, and dash-and-dotted lines show the variability of the solidification or melting effects in always the same encapsulated sample

(dash-and-dotted line) or even starting with a sharp leading edge and with a characteristic belly shaped finishing (full line); generating approximately the same transformation heat $\Delta H_b = -219.5 \pm 3.5 \text{ J g}^{-1}$. Independently of the freezing, the corresponding melting, being the quasi-equilibrium phase transition, proceeds always in the same way giving the endothermic peak with $T_{x,b} = 19.0 \pm 0.1 \text{ }^\circ\text{C}$ and $\Delta H_b = 222.2 \pm 3.5 \text{ J g}^{-1}$. The isothermic pre-annealing of the liquid at temperatures T_a close to $T_{x,b}$ accelerates its crystallization. The smaller is the overheating the earlier, i.e., at higher temperatures, the sample manifests the exotherm of solidification in the following cooling regime. The peak is only of the sharp leading edge and characteristic belly shaped finishing type, however, it slightly broadens, decreasing its depth; ΔH_b again does not show any measurable change (Fig. 2). The pre-annealing effect presented in Fig. 2 is typical for the pre-nucleation effect in the nucleation-and-growth kinetics [3, 4], therefore, it suggests the interpretation for the variability in the solidification cetane peak from Fig. 1. Thus, the soft peaks should represent the complete nucleation-and-growth within the DSC exotherm; while the sharp leading edge and characteristic belly shaped finishing type peaks might correspond only to the growth of the previously nucleated sample. The shift in $T_{x,b}$ should be related to the type of nucleation. Namely, the sample can nucleate heterogeneously (at higher temperatures $T_{x,b}$) due to the performance of eventual impurities or compositional disturbances within the volume of the liquid sample (the phenomenon has been observed even in the pure Au standard and it modified its crystallization by $200 \text{ }^\circ\text{C}$ [5]) or homogeneously (at lower $T_{x,b}$). Decreasing T_a to

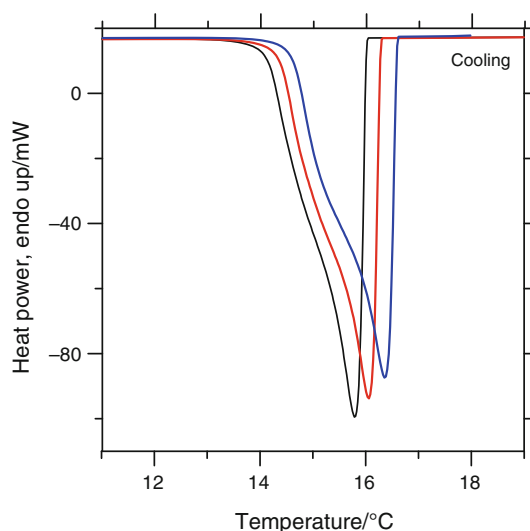


Fig. 2 Influence of the isothermal pre-annealing on the solidification of pure cetane. The cooling rate was $-2 \text{ }^\circ\text{C min}^{-1}$. DSC curves (from left to right) for as-produced cetane and for heat-treated samples at $20.9 \text{ }^\circ\text{C}$ for 170 min and at $18.9 \text{ }^\circ\text{C}$ for 240 min are shown. Always the same encapsulated sample was used

$18.4 \text{ }^\circ\text{C}$, the sample started to solidify already during the annealing after the incubation period $\tau = 107 \text{ min}$ and it completely crystallized after another 2 min. Modifying T_a , we were able to follow isothermally four crystallization exotherms. Figure 3 shows that, decreasing T_a , it means increasing the supercooling $\Delta T = 19 \text{ }^\circ\text{C} - T_a$, the incubation period τ decreases and the crystallization exotherm slightly narrows. If it was the Johnson–Mehl–Avrami kinetics (JMA) [6], the integral of the DSC signal $\alpha(t) = (\int_{\tau}^t y dv) / (\int_{\tau}^{t_{\text{end}}} y dv)$ (y is the DSC signal, v is the variable time, and t_{end} is the time of the end of the isothermal peak) should follow the relation (1) and the kinetic parameters n , being the Avrami exponent, and k , being the rate constant, might be calculated.

$$\ln[-\ln(1 - \alpha)] = n \ln k + n \ln t \quad (1)$$

The isothermal peaks from Fig. 3 were linearized for $0.1 < \alpha < 0.9$. The corresponding Avrami plots and the deduced parameters n and k are shown in Fig. 4. It is seen that the assumption of the JMA kinetics might be accepted (the coefficient of determination, $\delta^2 = 0.99$). The Avrami exponent approaching $n = 1.5$ suggests no nucleation and the diffusion controlled three-dimensional growth [6], a result which confirms our suggestive interpretation of the sharp leading edge and belly shaped finishing type of the solidification peaks. Further, it is evident that the rate constant k is temperature dependent, namely it increases with decreasing T . It means that it does not follow the traditional Arrhenius temperature dependence for the crystal growth or for the diffusion, $k(T) = A \exp(-E/RT)$, where A and E are the kinetic parameters and R is the gas

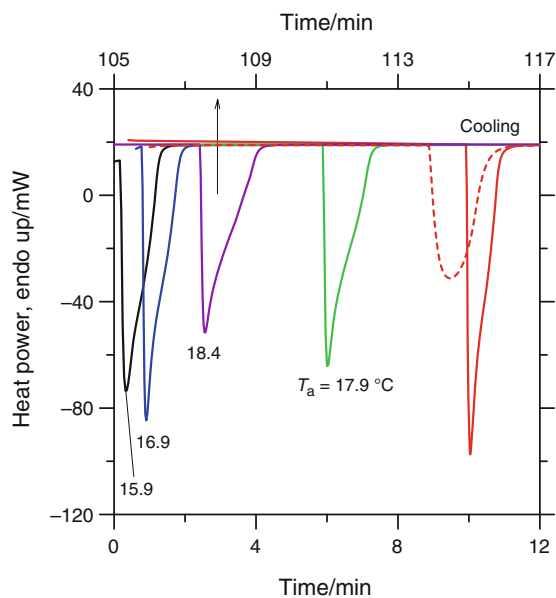


Fig. 3 Time scale representations of the solidification of pure cetane. Full and dashed red lines are for the continuous-cooling dependencies from Fig. 1. Other curves are for the isothermal measuring regime, where the annealing temperature is the parameter. The upper time scale is only for the 18.4 °C isotherm. Always the same encapsulated sample was used. (Color figure online)

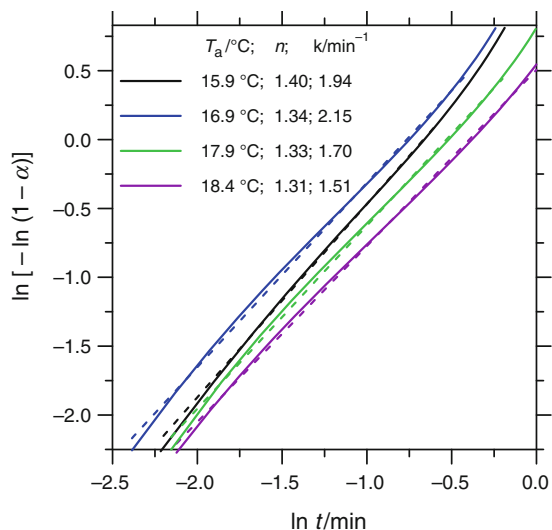


Fig. 4 JMA linearization of the DSC peaks from Fig. 3 for the isothermal solidification of pure cetane. Temperature of the isotherm, the slope being the Avrami exponent and the rate constant are shown in the legend

constant. Neither it is driven by the alternative relation for the nucleation $k(T) = A \exp[-E/(T\Delta T^2)]$ [7] even when the eventual nucleation has already been eliminated by the above-mentioned results. In any case, the anomalous solidification exotherm at $T_a = 16.9$ °C being too narrow, should be excluded from any analyzes.

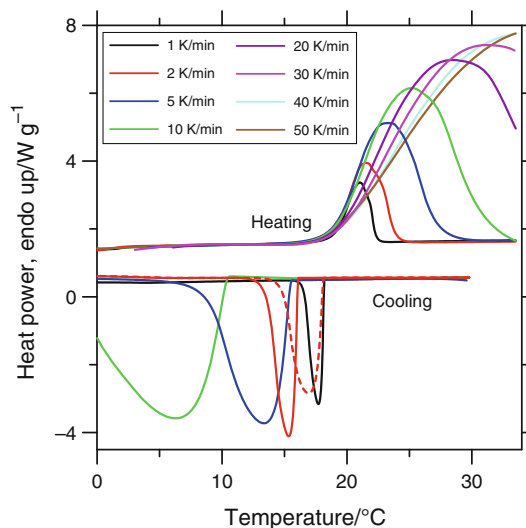


Fig. 5 Scanning rate dependence of the DSC cooling and heating curves for pure cetane. Always the same encapsulated sample was used

Further evidence about the kinetics of the complex solid/liquid transition in cetane is given by continuous heating and cooling regimes modifying the rate. It is seen in Fig. 5 that the heating rate does not affect the start of the melting; $T_{x,b}$ remains constant characterizing the equilibrium phase transition. Just the width of the peak, reflecting the thermal conductivity of cetane, increases proportionally to β . Oppositely, the increasing cooling rate enlarges the supercooling of the melt below the equilibrium melting temperature which conforms to the nucleation-and-growth crystallization.

After penetration of a cetane droplet in an open pore of silica gel, it wets the pore walls and its resulting surface curvature and also surface (or interfacial) tension depend on the contact angle θ and the pore radius r_p . Considering the solidification and melting effects for the quasi-equilibrium phase transitions, the thermal, chemical, and mechanical equilibria at the interfaces between the present gaseous, melt, and solid phases should exist. Thus, due to the modified surface (or interfacial) tension of the confined liquid also the new phase transition temperature $T_{x,c}$, different from the bulk (free) liquid one $T_{x,b}$, should exist. The simplified relation between the depression of the actual phase transition temperature and the radius of the confining pore r_p should follow the Gibbs–Thompson rule [2, 8]

$$T_{x,b} - T_{x,c} \sim B \cos\theta/r_p \quad (2)$$

where B is the material parameter.

In the case that the porous powder, after filling its pores with the liquid medium, contains also some excess liquid being in the bulk form (e.g., at the surface and in the space between the solid particles), both types of corresponding

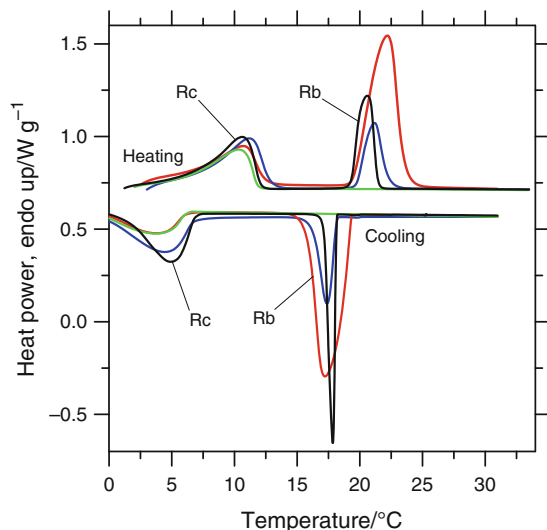


Fig. 6 DSC cooling and heating curves for cetane confined in silica gel having pores of 10 nm. Rb peaks represent the phase transition of bulk-cetane. Rc peaks represent the phase transition of confined-cetane. Red and green curves consecutively represent the same fresh and aged for 15 months encapsulated sample. Blue and black curves belong to always new batch of encapsulation. The scanning rates were $\pm 2 \text{ }^\circ\text{C min}^{-1}$. (Color figure online)

interfaces should exist. Therefore, the eventual solid/liquid phase transition of the liquid medium should take place separately in its bulk form (making a peak Rb at $T_{x,b}$) and in its confined form (making a peak Rc at $T_{x,c}$). Figure 6 shows such complex solidification and melting cycle for cetane in a silica gel. Cooling the sample the excess bulk-cetane crystallizes first at $T_{x,b} = 18.8 \pm 0.5 \text{ }^\circ\text{C}$ giving a relatively small peak Rb ($\Delta H_b = -20.7 \text{ J g}^{-1}$ of the sample). Its enthalpy, $\Delta H_b = -20.7 \text{ J g}^{-1}$, corresponds to the 9.4% of the overfilling cetane fraction. After supercooling by $T_{x,b} - T_{x,c} = 11.2 \text{ }^\circ\text{C}$, the confined-cetane starts to solidify forming a flat-and-broad peak Rc at $T_{x,c} = 7.7 \text{ }^\circ\text{C}$. The enthalpy of the peak is $\Delta H_c = -51.7 \text{ J g}^{-1}$ of the sample. This enthalpy corresponds to 23.6% of the confined-cetane fraction. During the next measuring step with heating the frozen sample, first the confined-cetane melts forming an isolated peak Rc at $T_{x,c} = 5.8 \text{ }^\circ\text{C}$ with $\Delta H_c = 50.5 \text{ J g}^{-1}$ of the sample. Finally, the melting of the minor bulk-cetane fraction (Rb) is observed at the equilibrium melting temperature $T_{x,b} = 19.4 \text{ }^\circ\text{C}$ and giving $\Delta H_b = 21.1 \text{ J g}^{-1}$ of the sample. Repeating the measurements in the time of 2 years, the Rb transformation peaks continuously loosed their power and finally they disappeared. Simultaneously, the enthalpy of the Rc transformation peak did not show any systematic modification. This effect and also the fact, that the sum of transformation heats of the bulk- and confined-cetane fractions is significantly smaller than the measured heat of the pure cetane (see Table 1), gives the reason to suggest that a third form of cetane should exist in the sample which

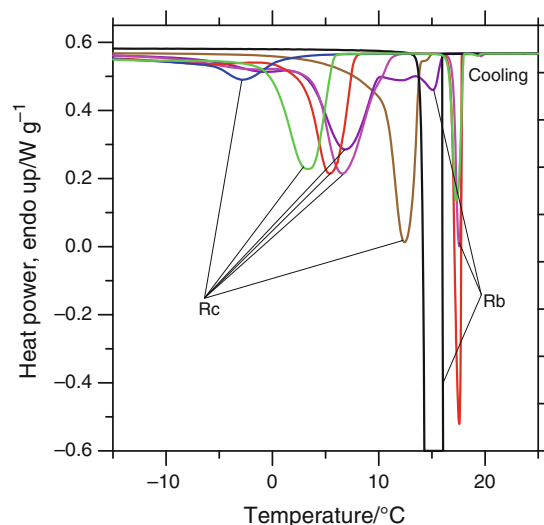


Fig. 7 DSC cooling curves for solidification of cetane confined in various silica gels: with 3 nm pores (blue line), with 6 nm pores (green line), with 10 nm pores (red line), with 12 nm pores (light violet line), with 15 nm pores (dark violet line), with 30 nm pores (brown line). The black line represents the bulk-cetane. Scanning rate was $-2 \text{ }^\circ\text{C min}^{-1}$. DSC8500 instrument with the intracooler up to $-80 \text{ }^\circ\text{C}$ was used. (Color figure online)

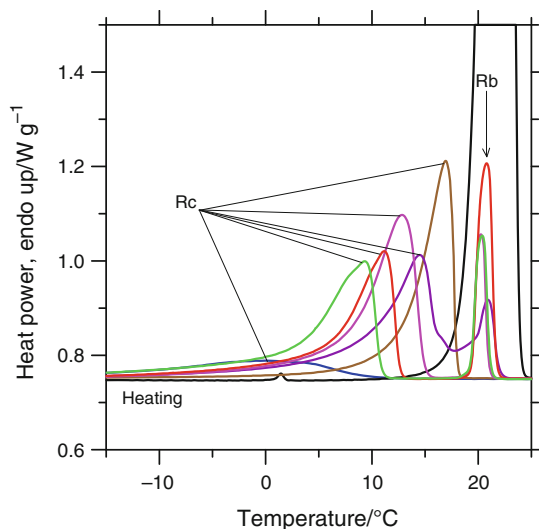


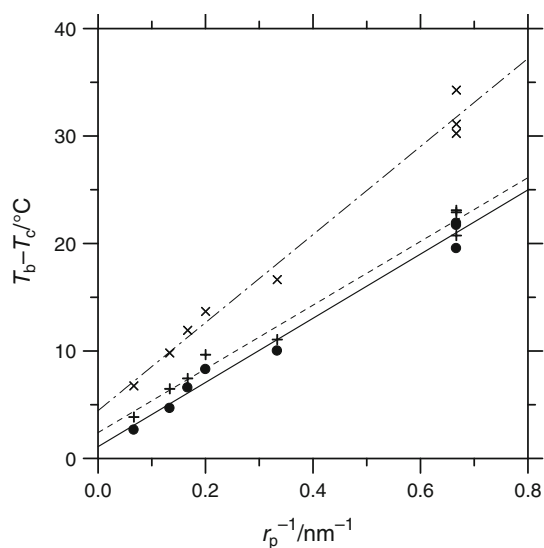
Fig. 8 DSC heating curves for melting of cetane confined in various silica gels: with 3 nm pores (blue line), with 6 nm pores (green line), with 10 nm pores (red line), with 12 nm pores (light violet line), with 15 nm pores (dark violet line), with 30 nm pores (brown line). The black line represents the bulk-cetane. Scanning rate was $+2 \text{ }^\circ\text{C min}^{-1}$. DSC8500 instrument with the intracooler up to $-80 \text{ }^\circ\text{C}$ was used. (Color figure online)

does not solidify during the DSC experiments. The search for such possibility will be the subject of our future investigation.

The fact that the Rc effect is essentially related to the phase transition of the confined-cetane and that it depends on the morphology of the hosting silica gel is proven in Figs. 7 and 8. Figures show the DSC curves for

Table 2 Thermodynamic properties of the melting of cetane confined in HPLC silica gels: mean pore diameter, onset, maximum and end of the DSC melting peak temperatures and transformation enthalpies of confined- and bulk-cetane forms. The heating rate was $+2\text{ }^{\circ}\text{C min}^{-1}$

d/nm	$T_{x,c}/^{\circ}\text{C}$	$T_{p,c}/^{\circ}\text{C}$	$T_{e,c}/^{\circ}\text{C}$	$T_{x,b}/^{\circ}\text{C}$	$T_{p,b}/^{\circ}\text{C}$	$T_{e,b}/^{\circ}\text{C}$	$\Delta H_c/\text{J g}^{-1}$	$\Delta H_b/\text{J g}^{-1}$
3	-14.69	0.02	9.05	–	–	–	25.5	0
4	3.37	9.19	10.82	–	–	–	52.6	0
6	2.68	9.3	10.83	19.31	20.36	21.20	55.0	11.7
10	5.76	11.14	12.59	19.43	20.79	21.62	50.5	21.1
12	7.47	12.81	14.88	19.39	20.25	20.92	64.4	10.2
15	9.32	14.46	16.61	19.13	20.93	21.91	56.0	12.4
30	12.84	16.93	17.97	–	–	–	54.5	0
∞	–	–	–	19.0	21.55	23.81	–	225.7

**Fig. 9** Melting temperature depression for cetane confined in silica gel as a function of reciprocal pore radius of the confining matrix. The symbols are for $T_{x,b} - T_{x,c}$ (multiplication symbol), $T_{p,b} - T_{p,c}$ (plus symbol), and $T_{x,b} - T_{p,c}$ (filled circle) data. The lines represent least-square linear regression fits to experimental data

solidification (Fig. 7) and subsequent melting (Fig. 8) of cetane in various silica gels. There, always the Rc peak is present. Its position ($T_{x,c}$) varies with the average pore radius following Eq. 2 taking part at lowest temperatures for the smallest pores. Its gain (ΔH_c) reflects the total pore volume; and its shape is related to the actual pore size distribution [2, 9]. On the other side, the Rb peak proceeds always at the same temperatures as in the case of the pure cetane (also shown in Figs. 7, 8), however, it is small and it needs not to exist always reflecting the eventual presence or absence of the excess cetane, e.g., the bulk-cetane form. The DSC curves taken in the cooling regime are more sensitive than the curves taken in the heating regime; however, they are influenced by the variability in the nucleation kinetics of the Rb peak, a fact which has already been discussed in the case of pure cetane.

The characteristic temperatures and enthalpies for the melting of both confined- and bulk-cetane forms are summarized in Table 2. The $T_{x,b} - T_{x,c}$ versus $1/r_p$ linear dependencies, being the “calibration” plots for the cetane thermoporometry, are shown in Fig. 9. Three combinations of the onset and maximum temperatures of the DSC peaks were tested. As plotted in Fig. 9, linear regression fits to the data provide the following expressions

$$T_{x,b} - T_{x,c} = 40.9807/r_p + 4.44448, \quad \sigma^2 = 2.15 \quad (3)$$

$$T_{x,b} - T_{p,c} = 29.8688/r_p + 1.09508, \quad \sigma^2 = 1.10 \quad (4)$$

$$T_{p,b} - T_{p,c} = 29.6657/r_p + 2.39792, \quad \sigma^2 = 1.16 \quad (5)$$

While following the recommendation of ICTAC, the onset temperatures are the most correct characterizations of the DSC peaks, the higher resolution of their maximums provided better residual mean squares σ^2 . The found dependences of $T_{x,b} - T_{x,c}$ versus $1/r_p$ are dramatic. Therefore, the temperature shifts for materials with large pores (being small) are bigger than in the case of water (being the most recommended liquid medium for the DSC thermoporometry) and larger pores can be searched. Moreover, the heat of fusion of cetane is not small (222 J g^{-1}), however, it is smaller than in the case of water (334 J g^{-1} , [1, 2]); the corresponding DSC peaks are smaller and, therefore, higher scanning rates can be used. Thus, the resolution of the shallow peaks will increase and the smaller pores might be searched. Thus, it can be concluded that cetane is an applicable medium for the eventual cetane thermoporometry.

Conclusions

In contrast to the single first-order phase transition, two effects have been observed, giving indication for the existence of minimally two forms of cetane. They should be the originally bulk- and the confined-forms. The connection between the properties of these two forms has been

searched. The thermodynamic characterization of the confined-cetane has been presented. The relation between the temperature of the complex melting of cetane and the dimensions of the pores in the confining matrix has been obtained. Cetane has been found to be a suitable probe liquid for determination of the average dimension of the pores in silica gels.

Acknowledgements Support of the Agency of the Ministry of Education of the Slovak Republic for the Structural Funds of the EU (CEKOMAT II, ITMS 26240120020) is gratefully acknowledged. The research was supported also by the projects VEGA 2/0111/11, 2/0171/09, 2/0099/10 and APVV—0647-10.

References

1. <http://en.wikipedia.org/wiki/Hexadecane>; http://en.wikipedia.org/wiki/Silica_gel. 21 Nov 2011.
2. Landry MR. Thermoporometry by differential scanning calorimetry: experimental considerations and applications. *Thermochim Acta*. 2005;433:27–50.
3. Chen LC, Spaepen F. Analysis of calorimetric measurements of grain growth. *J Appl Phys*. 1991;69:679–88.
4. Illeková E, Kuhnast FA, Maňko I, Naguet CH. Influence of preannealing on the crystallization of Fe₇₅Si₁₅B₁₀ metallic glass. *Mat Sci Eng A*. 1996;215:150–6.
5. Wilde G, Sebright JL, Perepozko JH. Bulk liquid undercooling and nucleation in gold. *Acta Mater*. 2006;54:4759–69.
6. Christian JW. The theory of transformations in metals and alloys. New York: Pergamon Press; 1965.
7. Suñol JJ, Farjas J, Berlanga R, Saurina J. Thermal analysis of a polyethylene glycol (PEG 4000): T-CR-T diagram construction. *J Therm Anal Calorim*. 2000;61:711–8.
8. Riikonen J, Salonen J, Lehto VP. Utilising thermoporometry to obtain new insights into nanostructured materials. Review part 1. *J Therm Anal Calorim*. 2011;105:811–21.
9. Riikonen J, Salonen J, Lehto VP. Utilising thermoporometry to obtain new insights into nanostructured materials. Review part 2. *J Therm Anal Calorim*. 2011;105:823–30.